Mitochondrial transcription factor A promotes DNA strand cleavage at abasic sites

Wenyan Xu (许文彦)[a,1], Riley M. Boyd[a,1], Maya O. Tree[a], Faris Samkari[a], and Linlin Zhao[a,b,2,3]

[a]Department of Chemistry and Biochemistry, Central Michigan University, Mount Pleasant, MI 48859; and [b]Biochemistry, Cellular, and Molecular Biology Graduate Program, Central Michigan University, Mount Pleasant, MI 48859

Edited by Rafael Radi, Universidad de la Republica, Montevideo, Uruguay, and approved July 18, 2019 (received for review July 2, 2019)

In higher eukaryotic cells, mitochondria are essential subcellular organelles for energy production, cell signaling, and the biosynthesis of biomolecules. The mitochondrial DNA (mtDNA) genome is indispensable for mitochondrial function because it encodes protein subunits of the electron transport chain and a full set of transfer and ribosomal RNAs. MtDNA degradation has emerged as an essential quality control measure to maintain mtDNA and to cope with mtDNA damage resulting from endogenous and environmental factors. Among all types of DNA damage known, abasic (AP) sites, sourced from base excision repair and spontaneous base loss, are the most abundant endogenous DNA lesions in cells. In mitochondria, AP sites trigger rapid DNA loss; however, the mechanism and molecular factors involved in the process remain elusive. Herein, we demonstrate that the stability of AP sites is reduced dramatically upon binding to a major mtDNA packaging protein, mitochondrial transcription factor A (TFAM). The half-life of AP lesions within TFAM–DNA complexes is 2 to 3 orders of magnitude shorter than that in free DNA, depending on their position. The TFAM-catalyzed AP-DNA destabilization occurs with nonspecific DNA or mitochondrial light-strand promoter sequence, yielding DNA single-strand breaks and DNA–TFAM cross-links. TFAM–DNA cross-link intermediates prior to the strand scission were also observed upon treating AP-DNA with mitochondrial extracts of human cells. In situ trapping of the reaction intermediates (DNA–TFAM cross-links) revealed that the reaction proceeds via Schiff base chemistry facilitated by lysine residues. Collectively, our data suggest a novel role of TFAM in facilitating the turnover of abasic DNA.

DNA damage | DNA turnover | DNA–protein cross-links | DNA repair | mitochondrial DNA degradation

Mitochondria are critical for energy production, cell signaling, and the biosynthesis of protein cofactors in higher eukaryotic cells (1, 2). Mitochondrial DNA (mtDNA), a double-stranded circular DNA of 16,569 bp, is present in multiple copies in mitochondria and exists in condensed DNA–protein complexes known as nucleoids. MtDNA encodes 13 protein subunits of the electron transport chain complexes and a full set of transfer and ribosomal RNAs, and is critically important for cellular function and organismal health (3–5). MtDNA is susceptible to endogenous and exogenous factors, resulting in mtDNA damage that can lead to mitochondrial genomic instability (3, 6), a contributor of the pathogenesis of various mitochondrial disorders, neurodegeneration, and cancer (7–9).

To cope with DNA damage, multiple repair pathways exist in mitochondria, with base excision repair (BER) being a major player (3, 7, 10). During BER, the oxidized or alkylated DNA lesions are excised enzymatically at the *N*-glycosidic linkage, forming abasic (AP) sites as an important intermediate. Subsequently, the AP lesion is repaired and replaced by an unmodified nucleotide via multiple enzymatic pathways (11, 12). AP sites are also produced by spontaneous loss of unmodified and alkylated nucleobases. Collectively, the total number of AP sites can range from 20,000 to 50,000 per cell each day, which makes AP sites the most abundant type of endogenous DNA damage in cells (13, 14). Within mitochondria, AP lesions are also abundant and can number in the hundreds per cell, considering their steady-state level (0.2 to 3 AP sites per 10^5 bp) (15, 16) and the number of mtDNA copies per cell (~1,000) (17). Importantly, AP sites are chemically labile and reactive and can lead to secondary DNA damage such as DNA single-strand breaks (SSBs), DNA–DNA interstrand cross-links, and DNA–protein cross-links (DPCs) (18–23). If not repaired, AP sites and their derivatives are mutagenic in the nuclear genome (24–26); however, the understanding of the biological consequence of AP sites in mitochondria remains limited.

Recently, mtDNA degradation has emerged as an essential mechanism to counteract mtDNA damage (27–35). MtDNA degradation is activated in response to difficult-to-repair DNA lesions or excessive DNA damage, and is thought to be nonspecific to DNA lesion types (27–32). Remarkably, Alexeyev and colleagues demonstrated that mitochondrial AP sites trigger mtDNA degradation in human and mouse cells (29, 36). The observed DNA loss is rapid and not likely due to autophagy, mitophagy, or apoptosis (30, 32). Collectively, this body of work underscores the importance of mtDNA degradation and suggests strongly the existence of unidentified pathways and molecular factors in this process.

In this work, we demonstrate that the stability of AP sites is reduced drastically when mitochondrial transcription factor A (TFAM) binds to an AP lesion-containing duplex DNA (AP-DNA). TFAM is a key protein that coats and packages mtDNA

Significance

Failure to maintain mitochondrial DNA (mtDNA) has been implicated in a variety of mitochondrial disorders and human diseases. mtDNA degradation is an important process for mtDNA maintenance and stress response; nevertheless, the mechanism by which mtDNA is degraded remains partially understood. We demonstrate that mitochondrial transcription factor A (TFAM) facilitates damaged DNA degradation by accelerating strand cleavage at abasic sites, reducing the half-life of abasic DNA by 2 to 3 orders of magnitude relative to free DNA. The TFAM-catalyzed AP-lesion destabilization occurs with nonspecific DNA or mitochondrial light-strand promoter sequence, facilitated by lysine residues of TFAM to form Schiff base intermediates. The catalytic effect of TFAM on abasic DNA suggests a novel role of TFAM in mtDNA metabolism.

Author contributions: L.Z. designed research; W.X., R.M.B., M.O.T., F.S., and L.Z. performed research; W.X., R.M.B., and L.Z. analyzed data; and L.Z. wrote the paper.

The authors declare no conflict of interest.

This article is a PNAS Direct Submission.

[1]W.X. and R.M.B. contributed equally to this work.

[2]To whom correspondence may be addressed. Email: linlin.zhao@ucr.edu.

[3]Present address: Department of Chemistry, University of California, Riverside, CA 92521.

This article contains supporting information online at www.pnas.org/lookup/suppl/doi:10.1073/pnas.1911252116/-/DCSupplemental.

Published online August 14, 2019.

molecules into nucleoids. TFAM binds to mtDNA specifically at promoter regions to activate mitochondrial transcription, and also nonspecifically throughout the mtDNA genome to condense mtDNA and regulate DNA transactions (37–40). Our study shows that recombinant human TFAM catalyzes the strand scission at AP sites, and decreases the half-life of AP lesions by 230- to 1,200-fold relative to free AP-DNA, depending on the position of AP sites. TFAM promotes the formation of Schiff base intermediates (i.e., DPCs) and SSBs, facilitated by several lysine residues. The TFAM-mediated AP-DNA destabilization occurs with both mitochondrial light-strand promoter (LSP) sequence or nonspecific DNA, and also when AP-DNA is treated with mitochondrial extracts of HeLa or HEK-293 cells. The importance of lysine residues in Schiff base formation and TFAM-mediated strand cleavage was confirmed using TFAM variants containing lysine residues substituted with alanine or arginine. Taken together, our results demonstrate that TFAM destabilizes abasic DNA, and suggest a novel role of TFAM in damaged mtDNA degradation.

Results

TFAM Accelerates Strand Scission at AP Sites with Nonspecific DNA. TFAM is a highly abundant protein in mitochondrial nucleoids that coats and compacts the entire mtDNA molecule. As a member of the high-mobility group (HMG) box proteins, TFAM contains two HMG-box domains and an interdomain linker (Fig. 1*A*), which together impose a U turn on mtDNA (37–39). By analysis of the X-ray crystal structures of TFAM–DNA complexes (37–39), we identified several lysine residues with the ε-NH_2 group close to the C1′-carbon of the nearby nucleotide residue (highlighted in purple in Fig. 1*A*). We hypothesized that the ε-NH_2 group of these lysine residues could act as a nucleophile and react with nearby AP sites via Schiff base chemistry to yield SSBs (Fig. 1*C*). To test this, we first determined the appropriate concentration of TFAM needed to form TFAM–DNA (1:1 molar ratio) complexes, which presumably conform to the reported structure (39). With a nonspecific DNA substrate similar to that used in previous structural work (39), the percent yield of TFAM–DNA (1:1) complexes is the highest when the two components are mixed at a 2:1 (TFAM/DNA) molar ratio according to electrophoretic mobility-shift assays (EMSAs; Fig. 2*A*). We thus adopted this ratio in our subsequent assays.

We carried out reactions with recombinant human TFAM and AP-DNA under physiological conditions (pH 7.4, 37 °C). On the basis of structural data (39), we designed an oligodeoxynucleotide with a deoxyuridine (dU) residue as the precursor of AP sites and a 3′-fluorescein (FAM) label. The dU residue was designed near the amino acid residue K69 in the TFAM–DNA structure, and the FAM label was used to follow the strand cleavage reaction. Uracil-DNA glycosylase was used to convert the dU residue to an AP lesion. The resulting AP-DNA (hereinafter referred to as AP_1; sequence shown in *SI Appendix*, Table S1) was mixed with TFAM at a 2:1 (TFAM/DNA) molar ratio to form TFAM–AP_1 complexes. After incubation for varying times, reaction aliquots were taken and quenched with the reducing agent $NaBH_4$ to minimize subsequent adventitious strand cleavage. We analyzed the reaction products using an SDS-urea gel to separate DNA and protein under denaturing conditions. As shown in Fig. 2*B*, AP_1 was quickly converted to SSBs over time (lane 6, 30-min reaction; lane 7, 12-h reaction). Aside from SSBs, in situ trapping with $NaBH_3CN$ produced slower-migrating bands (lanes 4 and 5), which are assigned as covalent TFAM–DNA cross-links based upon the fluorescence signal (from DNA), their molecular weight, and their conversion into faster-migrating products upon proteolytic digestion (*SI Appendix*, Fig. S4; vide infra). Successful trapping of DPCs with $NaBH_3CN$ suggests the formation of Schiff base intermediates and the involvement of TFAM in the reaction. The formation of

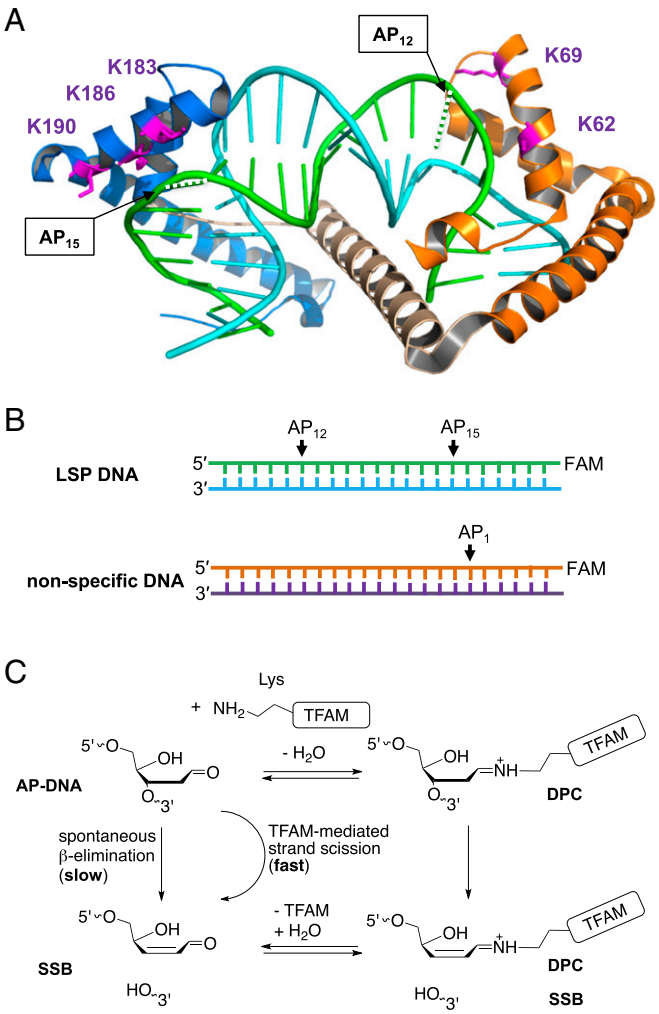

Fig. 1. Structural basis and proposed mechanism of TFAM-mediated DNA strand scission at AP sites. (*A*) Crystal structure of TFAM complexed with DNA containing the mitochondrial light-strand promoter sequence (PDB ID code 3TQ6). The two HMG-box domains of TFAM are in orange (HMG1) and blue (HMG2), and the interdomain linker is in wheat. Potentially reactive (with AP sites) lysine residues within the two HMGs are highlighted in purple. The heavy strand is in cyan, and the light strand is in green with the positions of AP lesions shown as dashed lines. (*B*) AP-DNA substrates with the positions of AP sites indicated by arrows. (*C*) The proposed mechanism of TFAM-catalyzed DNA strand cleavage at AP sites via Schiff base intermediates (DNA–protein cross-links) to form single-strand breaks.

SSBs was abolished in the presence of an AP site-reactive chemical, methoxyamine (Fig. 2*B*, lane 8), confirming the participation of AP sites in the reaction.

To assess the role of TFAM in AP-site destabilization, we determined the kinetics of the disappearance of AP_1 and the formation of SSBs and DPCs using denaturing polyacrylamide gel electrophoresis (PAGE) (Fig. 2*C* and *SI Appendix*, Fig. S4). The DPCs were converted to peptide–DNA cross-links by proteolytic (trypsin) digestion prior to gel electrophoresis to facilitate their migration (for simplicity, DPCs were used without specifying peptide–DNA cross-links). Quantifying the resulting products from denaturing PAGE analysis revealed the time course formation for all three components (Fig. 2*C*). In TFAM–AP_1 complexes, intact AP_1 underwent relatively rapid strand scission at AP sites, with only 20% of intact DNA remaining after a 24-h reaction. The rate of AP_1 disappearance was approximated by ignoring the reversibility of initial Schiff base

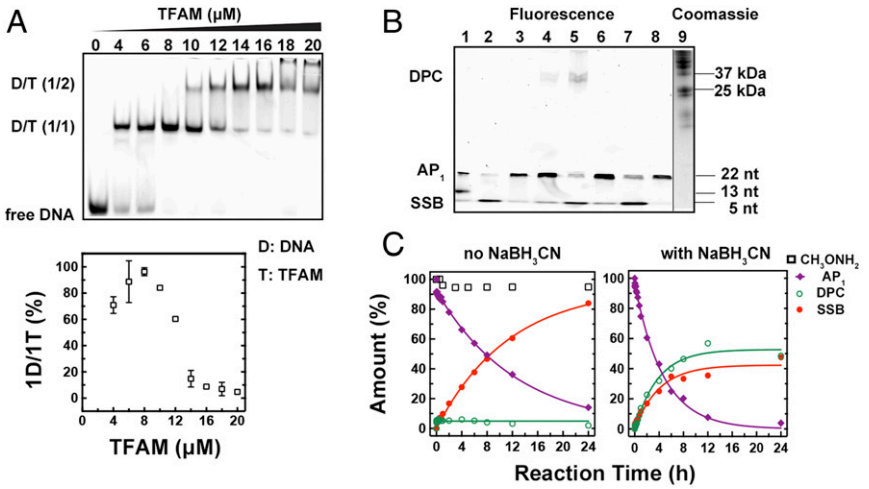

Fig. 2. TFAM accelerates strand cleavage at AP sites with nonspecific DNA. (*A*, *Top*) Representative electrophoretic mobility-shift analysis to determine the binding stoichiometry. (*A*, *Bottom*) The percent yield of 1D–1T complexes (D, DNA; T, TFAM). Data are from two independent experiments, and errors indicate the range of data. (*B*) TFAM induces the formation of DPCs and SSBs with AP_1 (AP-DNA with a nonspecific sequence), observed by SDS-urea PAGE. Lane 1, oligodeoxynucleotide markers; lane 2, confirmation of the presence of AP lesion in AP_1 after alkaline cleavage (0.1 M NaOH, 37 °C for 30 min); lane 3, stabilized AP_1 after reduction with 0.1 M $NaBH_4$; lanes 4 and 5, reactions of TFAM and AP_1 for 0.5 and 12 h, respectively, with DPCs trapped in situ by $NaBH_3CN$ (25 mM); lanes 6 and 7, reactions of TFAM and AP_1 for 0.5 and 12 h, respectively, without $NaBH_3CN$; lane 8, inhibition of DPC and SSB formation in the presence of the AP lesion-capping reagent methoxyamine (10 mM); lane 9, molecular mass ladder. (*C*) Representative time course of DPC and SSB formation, and AP-site disappearance, derived from denaturing PAGE analysis shown in *SI Appendix*, Fig. S4. Data from control reactions with methoxyamine are shown as black squares. Data were fit to a single-exponential decay equation to obtain the formation rate and half-life of AP_1.

formation (22) and fitting the data to a single-exponential decay equation to obtain a k_{dis} of 2.3×10^{-5} s^{-1} (Table 1). The half-life of AP sites within TFAM-bound AP_1 is 8.7 h, in stark contrast with a half-life of 980 h observed in free AP_1 (Table 1 and *SI Appendix*, Fig. S7). The 110-fold reduction in half-life supports strongly the role of TFAM in AP-lesion destabilization. Without chemical trapping, the reaction produced only a basal level (~3%) of DPCs in the first few hours (Fig. 2*C*, *Left* and Table 2). Reactions with methoxyamine (Fig. 2*C*, *Left*) abolished SSB and DPC formation, consistent with the results in Fig. 2*B*, lane 8. In situ trapping with $NaBH_3CN$ stabilized the Schiff base intermediates (DPCs) and caused a significant increase in the DPC yield (~50%) at the expense of SSBs (Fig. 2*C*, *Right*). Together, our results argue that the accelerated strand cleavage at AP sites depends on a TFAM-mediated Schiff base intermediate(s) and that the formation of DPCs is slow relative to the hydrolysis of the intermediate(s).

The Reactivity of AP Sites Varies Based on Their Position in TFAM–DNA Complexes. To examine the susceptibility of AP sites at different locations within DNA–TFAM complexes, we generated AP-DNA substrates using the LSP sequence. It is well-documented that TFAM binds to LSP-DNA with a defined conformation and polarity to activate transcription (37–40). Therefore, we used LSP-DNA substrates containing a specifically positioned AP lesion to probe the interactions of AP sites with surrounding amino acid residues. The duplex DNA with an AP lesion near K69 and K62 of HMG1 is referred to as AP_{12}, and that with an AP lesion near K183, K186, and K190 of HMG2 is referred to as AP_{15} (graphic illustration shown in Fig. 1; sequence shown in *SI Appendix*, Table S1).

When AP_{15} is complexed with TFAM, rapid strand scission at AP sites was observed within minutes, leaving only ~10% intact DNA after an 8-h incubation (Fig. 3, *Left* and *SI Appendix*, Fig. S5). Fitting the time course of AP_{15} disappearance to a single-exponential decay function yields a rate of disappearance of 8.1×10^{-5} s^{-1} (Table 1). The half-life of AP sites within TFAM–AP_{15} complexes is only 2.4 h, a dramatic decrease compared with a $t_{1/2}$ of 2,800 h in naked AP_{15} (Table 1 and *SI Appendix*, Fig. S7). The 1,200-fold reduction in the half-life of AP sites corroborates our observations with nonspecific DNA, and again points to a role of TFAM in AP-DNA destabilization. To confirm further that the observed effect is not due to TFAM simply supplying free amino groups, we conducted reactions with N_α-acetyl-lysine and AP_{15} mixed at a 2:1 molar ratio. In this case, the rate of disappearance (6.8×10^{-7} s^{-1}) is 2 orders of magnitude lower than that of TFAM-catalyzed reactions, indicating that the observed destabilization of abasic DNA is indeed due to specific interactions between TFAM and AP sites. In the presence of $NaBH_3CN$ (Fig. 3, *Right* and *SI Appendix*, Fig. S5), faster strand cleavage was observed, likely because the stabilized

Table 1. Effect of wild-type TFAM in promoting strand cleavage at AP sites in TFAM–DNA complexes

	TFAM–DNA complex				
AP-DNA	$NaBH_3CN$	k_{dis}, 10^{-5} s^{-1}	$t_{1/2}$, h	Free DNA $t_{1/2}$, h	Fold reduction in $t_{1/2}$ relative to free DNA
AP_1	–	2.3 ± 0.4	8.8 ± 1.6	980 ± 120	110
AP_1	+	7.2 ± 1.3	2.7 ± 0.4	–	
AP_{15}	–	8.1 ± 1.1	2.4 ± 0.3	2,800 ± 100	1,200
AP_{15}	+	29 ± 1	0.67 ± 0.004	–	
AP_{12}	–	9.1 ± 0.7	2.1 ± 0.2	480 ± 50	230
AP_{12}	+	12 ± 1.4	1.6 ± 0.05	–	

The rates of AP-lesion disappearance were obtained by fitting data to a single-exponential function. Data are mean ± SD ($n = 3$).

Table 2. Importance of lysine residues in forming DPCs and SSBs with AP-DNA in TFAM–DNA complexes

TFAM–DNA complexes	$NaBH_3CN$	DPC formation rate k_f, 10^{-5} s^{-1}	DPC yield, %	AP-lesion disappearance k_{dis}, 10^{-5} s^{-1}	$t_{1/2}$, h
WT–AP_1	–		3.0 ± 2.7	2.3 ± 0.4	8.8 ± 1.6
	+	7.3 ± 0.8	62 ± 16	7.2 ± 1.3	2.7 ± 0.4
WT–AP_{15}	–		2.6 ± 1.2	8.1 ± 1.1	2.4 ± 0.3
	+	24 ± 2	56 ± 9	29 ± 1	0.67 ± 0.004
3KA–AP_{15}	–		1.5 ± 0.7	6.6 ± 1.3	3.0 ± 0.6
	+	12 ± 2	30 ± 2	11 ± 0.03	1.8 ± 0.01
3KR–AP_{15}	–		1.5 ± 0.8	5.8 ± 0.9	3.4 ± 0.5
	+	6.7 ± 3.0	45 ± 12	8.9 ± 1.9	2.5 ± 0.6
WT–AP_{12}	–		1.3 ± 0.5	9.1 ± 0.7	2.1 ± 0.2
	+	11 ± 0.7	30 ± 8	12 ± 1.4	1.6 ± 0.05
2KA–AP_{12}	–		N/A	6.2 ± 0.1	3.1 ± 0.03
	+	6.1 ± 0.5	30 ± 1	7.0 ± 0.1	2.7 ± 0.1

The rates of DPC formation and AP-lesion disappearance were obtained by fitting data to a single-exponential function. Data are mean ± SD (n = 3). N/A, not detected using ImageQuant software.

DPC intermediates disrupt the reversibility of Schiff base formation and promote the forward reaction. The yield of DPCs was increased significantly (~60% in 2 h) at the expense of SSBs (Table 2). In composite, our data demonstrate that AP lesions formed near K183, K186, and K190 within HMG2 are highly susceptible to strand cleavage by TFAM.

We also examined the lability of AP sites near K69 and K62 using AP_{12}, and found that AP sites in AP_{12} appear to be less labile compared with that in AP_{15}. First, we used the reduction (relative to free DNA) in the half-life of AP sites to compare effects of the lysine residues within the two HMG domains, because the half-life of AP sites is sequence-dependent (41, 42). As shown in Table 1, when compared with the 1,200-fold reduction of AP-lesion half-life in AP_{15}, the 230-fold reduction observed with AP_{12} indicates that AP sites near K69 and K62 in HMG1 are less labile, albeit still much more labile than in free DNA. Second, we compared the relative increase in the rate of AP-DNA disappearance with and without chemical trapping (Table 2). Chemical trapping of DPCs in situ resulted in a nearly 4-fold increase in the rate of AP-DNA disappearance with AP_{15} (8.1 vs. 29×10^{-5} s^{-1}), whereas an only marginal increase was observed for AP_{12} (9.1 vs. 12×10^{-5} s^{-1}), suggesting the formation rate of DPCs contributes differently to the overall reaction in HMG1 and HMG2. A faster DPC formation rate observed with AP_{15} (24×10^{-5} s^{-1}) relative to AP_{12} (11×10^{-5} s^{-1}) under $NaBH_3CN$ trapping also corroborates these data (Table 2). These differences are consistent with the fact that potentially more lysine residues (K183, K186, and K190) within HMG2 contribute to the reaction as compared with HMG1 (K69 and K62). Overall, the results demonstrate that TFAM destabilizes AP sites and promotes strand cleavage in TFAM–DNA complexes. The role of TFAM in reducing the stability of AP sites resembles that of histone proteins; however, the extent of reduction in AP-lesion half-life appears to be more dramatic than that observed in nucleosome core particles (22, 43).

Lysine Residues of TFAM Contribute to Rapid Strand Scission at AP Sites. On the basis of structural analysis, we hypothesized that lysine residues (K183, K186, and K190 in HMG2; K62 and K69 in HMG1; shown in Fig. 1*A*) play a role in TFAM-mediated AP-DNA strand scission. To test this, we prepared variant forms of TFAM, containing K183A/K186A/K190A (3KA), K183R/K186R/K190R (3KR), and K62A/K69A (2KA). We paired 3KA or 3KR with AP_{15}, and 2KA with AP_{12}, to compare the effect of the variant proteins in AP-lesion destabilization relative to wild-type (WT) TFAM. Substituting lysine with alanine is expected to abolish the Schiff base intermediates derived from these residues, whereas substitution with arginine (a weaker nucleophile under physiological pH) is expected to diminish the formation of DPCs. To ensure similar TFAM–DNA complexes are formed with variant proteins, we performed EMSA to verify the binding stoichiometry. As observed in *SI Appendix*, Fig. S3, relative to WT TFAM, the binding patterns of variants were nearly identical, with either LSP-DNA or tetrahydrofuran-containing DNA (THF-DNA; THF is a stabilized AP-lesion analog). These results confirm that neither the amino acid substitution nor the presence of AP sites alters the binding stoichiometry of TFAM with DNA, though a slight increase in $K_{d,DNA}$ was observed with the K-to-A variants (*SI Appendix*, Fig. S2). On the other hand, the 3KR variant maintains similar DNA-binding affinity relative to WT ($K_{d,DNA}$, 6.7 ± 0.7 nM), as indicated by a $K_{d,DNA}$ of 8.4 (±1.0) nM, ensuring that the K-to-R substitution has minimal impact on the TFAM–DNA interactions (*SI Appendix*, Fig. S2*D*).

In the presence of chemical trapping, the 3KA variant compromised the DPC formation with AP_{15} significantly (Fig. 4*A*,

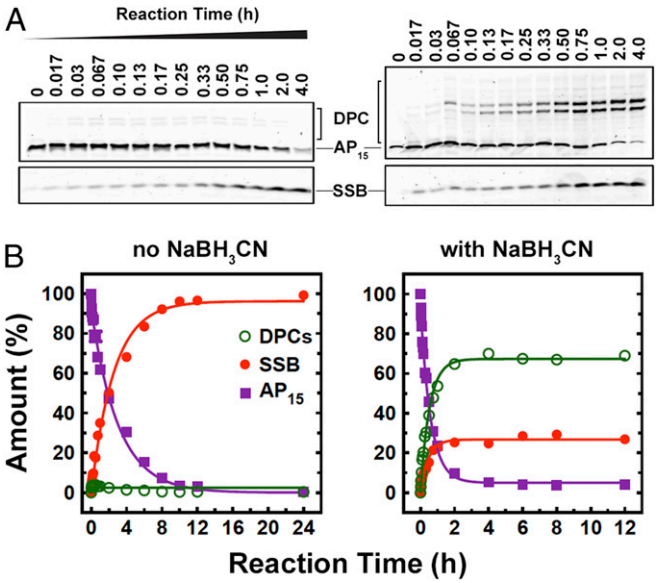

Fig. 3. TFAM facilitates strand scission at AP sites with LSP-DNA (AP_{15}). (*A*) Representative denaturing PAGE analysis of reactions of TFAM with AP_{15}. (*B*) Fitting the time course to a single-exponential function to extract the rates of DPC and SSB formation and AP_{15} disappearance (summarized in Table 2).

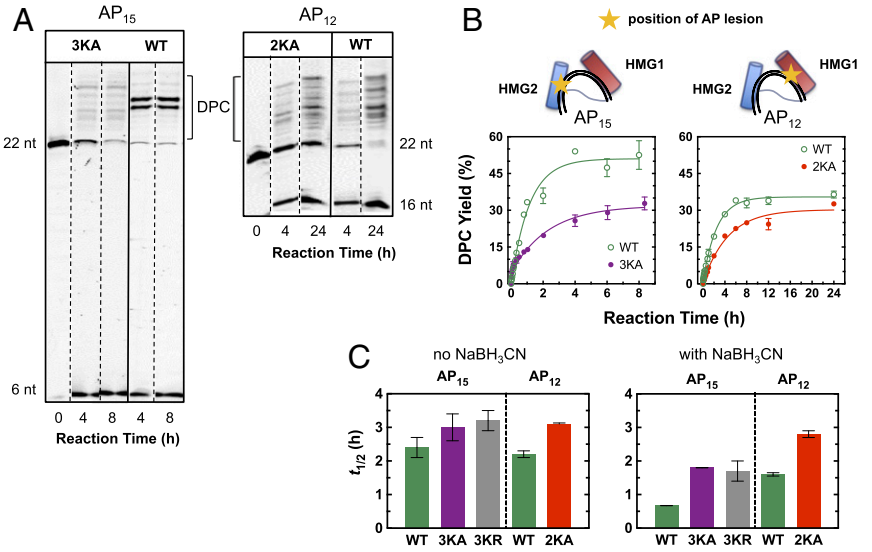

Fig. 4. Importance of lysine residues in AP-lesion destabilization. (*A*) Representative denaturing PAGE analysis of the reaction products with wild-type TFAM and variants in the presence of $NaBH_3CN$. The complete images are shown in *SI Appendix*, Figs. S5 and S6. (*B*) Relative to wild-type TFAM, TFAM variants with lysine-to-alanine substitutions show slower DPC formation rates. DPCs are trapped by reducing the C=N to C–N with $NaBH_3CN$. Data are mean ± SD ($n = 3$). (*C*) Effect of lysine-to-alanine substitution on the half-life of AP_{12} and AP_{15}. Data are mean ± SD ($n = 3$).

Left and *SI Appendix*, Fig. S5). Fitting the reaction time course to a single exponential equation revealed a nearly 50% decrease in the yield (WT, 56%; 3KA, 30%) and the formation rate of DPCs (WT, 24×10^{-5} s^{-1}; 3KA, 12×10^{-5} s^{-1}), as shown in Fig. 4*B* and Table 2. The observation confirms the importance of the three lysine residues in HMG2 in Schiff base formation. Notably, the 3KA variant did not completely abolish the DPC formation (Fig. 3*A* and *SI Appendix*, Fig. S5), suggesting that in the absence of the three lysine residues, additional amino acid residues could contribute to the DPC formation. As expected, reactions with AP_{15} and 3KR revealed an ∼20% decrease in the DPC yield (WT, 56%; 3KR, 45%) and an ∼75% decreased formation rate (WT, 24×10^{-5} s^{-1}; 3KR, 6.7×10^{-5} s^{-1}; Table 2), reinforcing the importance of K183, K186, and K190. Although the 45% DPC yield with 3KR is greater than the 30% yield with 3KA as expected, the DPC formation rate is similar with the two variants (6.7 [±3.0] vs. 12 [±2] $\times 10^{-5}$ s^{-1}) considering the SE of the experiments, likely due to a differing DPC formation mechanism by other lysine or arginine residues in the two variants. On the other hand, substitutions of K62A and K69A (2KA–AP_{12} complexes) resulted in a similar overall DPC yield (∼30%), albeit formed at a slower rate (6.1×10^{-5} s^{-1}) relative to reactions with WT TFAM (11×10^{-5} s^{-1}), as shown in Table 2, Fig. 4*A* (*Right*), Fig. 4*B* (*Right*), and *SI Appendix*, Fig. S6. These data suggest that lysine or arginine residues other than K62 and K69 participate in the Schiff base formation. Overall, the observation that TFAM variants did not eliminate the imine formation correlates with the known conformational flexibility of TFAM–DNA complexes (44). Not surprisingly, relative to WT TFAM, reactions with each of three TFAM variants (3KA, 3KR, and 2KA) led to an increase in the half-life of AP sites (Fig. 4*C*), indicative of the importance of the lysine residues in the AP destabilization. Collectively, the results verify the importance of putative lysine residues in HMG1 and HMG2 for accelerated strand scission with AP-DNA.

TFAM–DNA Cross-Links Form with Mitochondrial Extracts of Human Cells. To demonstrate that TFAM-promoted strand cleavage can occur in the presence of other mitochondrial proteins, we prepared mitochondrial extracts from HeLa and HEK-293 cells and conducted similar reactions with AP_{15} using $NaBH_3CN$ to trap the DPC intermediates. After a 1-h incubation at 37 °C, Western blotting analysis using TFAM antibody revealed supershifted TFAM conjugates corresponding to products formed with AP_{15} and recombinant TFAM (*SI Appendix*, Fig. S8*A*). Relative to wild-type HeLa cells, experiments with mitochondrial extracts from TFAM-knockdown cells (confirmed by Western blotting; Fig. 5*A*, lanes 1 and 2) showed a substantially lower yield of DPCs (Fig. 5*A*, lane 4), reinforcing the importance of TFAM in the cross-linking reaction. Because AP endonuclease APE1 plays an essential role in AP-lesion repair and is known to localize to mitochondria (45), we assayed the APE1 activity using a THF-containing substrate (AP_{15}-THF). The assay captures the specificity of APE1 in cleaving the THF-containing substrate (46, 47), whereas TFAM and other glycosylases do not have strand-scission activities with this substrate. As shown in Fig. 5*B*, APE1 in mitochondrial extracts of HeLa cells cleaves AP_{15}-THF and produces a 6-nt DNA fragment, correlating with the reaction product formed by recombinant APE1. Similar results were obtained with mitochondrial extracts from HEK-293 cells (*SI Appendix*, Fig. S8). These data demonstrate clearly that TFAM interacts strongly with AP-DNA to form DPC intermediates in the presence of other mitochondrial proteins, and at physiologically relevant concentration ratios of TFAM and APE1 in human cells.

To demonstrate quantitatively that TFAM is able to compete with APE1, we purified and assayed the recombinant human APE1 (*SI Appendix*, Fig. S1). The recombinant APE1 is highly active, as evidenced from its DNA binding ($K_{d,DNA}$, 0.61 nM in *SI Appendix*, Fig. S2) and strand-scission activities (Fig. 5 *B* and *C* and *SI Appendix*, Fig. S9). Considering that none of the BER factors including APE1 has been identified as a mitochondrial nucleoid protein (48, 49), the steady-state concentration of APE1 in mitochondria is likely to be very low. We carried out competition assays under varying molar ratios of DNA/APE1 (i.e., 1,000, 100, and 10) and titrated TFAM in the APE1-mediated AP_{15}-THF strand-scission reactions. TFAM shows an inhibitory effect under all three conditions (Fig. 5 *C* and *D* and *SI Appendix*, Fig. S9). At molar ratios of 100 and 1,000 (TFAM/APE1), the extracted relative IC_{50} values correlate well with the physiological concentration ratios of TFAM and mtDNA (50, 51), suggesting the possibility that TFAM may complement AP lyases in vivo. In summary, the combined data from experiments with mitochondrial extracts and those with recombinant APE1 argue that TFAM interacts strongly with

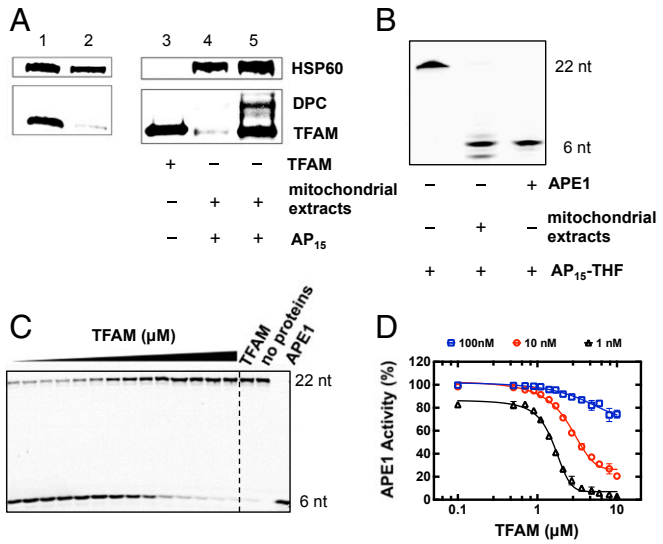

Fig. 5. Formation of DPCs in reactions of AP_{15} with mitochondrial extracts from HeLa cells and in the presence of APE1. (*A*) Western blotting analysis of TFAM levels and reaction products of AP_{15} with mitochondrial extracts from HeLa cells. HSP60 (mitochondrial heat shock protein 60 kDa) was used as a loading control. Lanes 1 and 2, TFAM levels in mitochondrial extracts from wild-type HeLa cells and HeLa cells after stable TFAM knockdown. Lane 3, recombinant human TFAM. Lanes 4 and 5, reactions of AP_{15} with mitochondrial extracts from TFAM-knockdown cells and wild-type HeLa cells, respectively. DPC is confirmed by Western blotting as well as its migration relative to the products obtained with AP_{15} and recombinant TFAM (a representative image is shown in *SI Appendix*, Fig. S8*A*). The detailed reaction condition is described in *Materials and Methods*. (*B*) APE1 is active in the mitochondrial extracts from HeLa cells. The AP lyase activity of APE1 is assayed using an AP_{15}-THF substrate. The cleaved product was assigned by comparing with the products obtained with reactions using recombinant APE1. (*C*) A representative image from PAGE analysis demonstrating the inhibitory effect of TFAM toward the AP lyase activity of APE1. Reactions contained 1 μM AP_{15}-THF, 1 nM APE1, and varying concentrations of TFAM. PAGE analysis for reactions with 10 and 100 nM APE1 is shown in *SI Appendix*, Fig. S9. (*D*) Fitting the TFAM inhibition data to an inhibitor dose–response equation (described in *Materials and Methods*) to extract the relative IC_{50} values under different conditions. Data in the graph are from 2 independent experiments, and errors indicate the range of data. IC_{50} values were 1.6 ± 0.05 μM in the presence of 1 nM APE1, 2.7 ± 0.07 μM in the presence of 10 nM APE1, and 5.1 ± 1.3 μM in the presence of 100 nM APE1. Data are mean (n = 2) ± SE of the fitting.

AP-DNA to form a Schiff base intermediate(s) and, considering the abundance of TFAM in nucleoids, that TFAM-mediated AP-DNA cleavage is likely to occur.

Discussion

Importance of mtDNA Degradation. The degradation of mtDNA has been documented since the 1960s (27, 28, 52–54). In unstressed rat tissues, mtDNA has a half-life of a matter of days, much shorter than that of nuclear DNA (52). In response to DNA-damaging agents or replication inhibitors, mitochondria can discard damaged DNA molecules to maintain mitochondrial function (27, 28, 53, 54). The degradation is believed to be nonspecific to lesion types and to be activated either when mitochondria are unable to repair specific lesions or when the number of lesions exceeds the repair capacity (27–32). mtDNA degradation may also contribute to the etiology of mtDNA depletion syndromes (55, 56), and to the activation of the innate immune system by circulating mtDNA (57, 58). The idea of a "disposable genome" (31) has inspired emerging research in gene therapy to selectively eliminate the pathogenic mtDNA molecules in mtDNA diseases (59–62).

TFAM Promotes Strand Cleavage at AP Sites. Previous work has shown that mtDNA elimination counteracts the mutagenicity of AP sites in human and mouse cells, as evidenced by a decline in mtDNA copy number and a moderate mutation load after the induction of mitochondrial AP sites (36). Nonetheless, the chemical and molecular basis of AP-DNA elimination remains an important unsolved question. In this study, we present compelling data demonstrating that TFAM promotes DNA strand scission at AP sites. The AP lesion is chemically labile and can undergo slow decomposition with a half-life on the order of weeks (22); however, TFAM significantly reduces the AP-site half-life by 2 to 3 orders of magnitude, producing strand breaks in minutes (Table 1). We confirmed that several lysine residues (K62, K69, K183, K186, and K190) in the two high-mobility group domains of TFAM promote the strand scission, and facilitate Schiff base formation. Interestingly, the observation that lysine-to-alanine substitution did not completely abolish the DPC formation suggests a potential role of other lysine or arginine residues in promoting strand scission at AP sites. The TFAM–LSP-DNA complexes have been shown to be dynamic rather than static structures (44). On the basis of structural analysis, we reason that other lysine (e.g., K76) or arginine (e.g., R59) residues in TFAM variants could contribute to the reaction by interacting transiently with AP sites through a butterfly-like TFAM–DNA complex breathing (44). Also, considering the flexibility of the interdomain linker, lysine or arginine residues in the linker region could potentially contribute to the observed reaction in TFAM variants (44). The potential for multiple residues to contribute to the AP-DNA strand cleavage, and the fact that TFAM coats the entire mtDNA molecule, suggests a ubiquitous nature of the TFAM-promoted AP-DNA degradation, regardless of the position of the AP lesion.

Considering the abundance of both TFAM and of AP sites, and the fact that TFAM slides along the DNA (63), it appears inevitable that TFAM would encounter endogenous AP sites in mitochondria. Our combined data suggest a novel role for TFAM in facilitating strand scission at AP sites, which may aid in the degradation of damaged DNA molecules. Research to validate such a role in human cells is currently ongoing. Meanwhile, two recent papers have reported the importance of several enzymes in linear mtDNA degradation, including DNA polymerase γ, helicase TWINKLE, and exonuclease MGME1 (64, 65). Whether TFAM-mediated AP-DNA degradation complements the removal of linear mtDNA by these enzymes warrants further investigation.

Implications of the Role of TFAM in DNA Repair. A model in which the association of TFAM with DNA inhibits BER activities was proposed earlier based on in vitro inhibition of several BER enzymes in the presence of TFAM (66). The authors also speculated that TFAM might not inhibit DNA repair in vivo (66). Our observation that TFAM promotes strand cleavage at AP sites suggests an active role of TFAM in processing ubiquitous AP sites, which may account for the rapid DNA depletion resulting from mitochondrial AP sites (36). Such strand cleavage activity may also act redundantly with APE1 or bifunctional glycosylases in their strand-scission activities. Three key factors are likely to play a vital role in determining the equilibrium between DNA packaging and repair. First, the regulation of TFAM copy number by Lon protease (67) may create DNA-binding sites for other repair enzymes. Second, the posttranslational modifications of TFAM can modulate its DNA-binding activity (68, 69), which may allow the access of repair enzymes. Third, potential protein–protein interactions between TFAM and other repair enzymes, which remain poorly understood, may also regulate DNA repair pathways.

In summary, although mtDNA degradation has been recognized as a pivotal mechanism for mitochondrial genome maintenance, the chemical and molecular mechanisms of the process

remain enigmatic. Our finding documents an emerging role of TFAM in the degradation of damaged mtDNA molecules, and provides a biochemical foundation for further exploring the role of TFAM in mtDNA turnover.

Materials and Methods

Materials. Commercial chemicals were from Sigma-Aldrich or Research Products International, and were of the highest quality available. *Escherichia coli* BL21 (DE3) competent cells and uracil DNA glycosylase (UDG) were from New England Biolabs. The pET28a vector expressing the mature form of full-length human TFAM (amino acids 43 to 246) was a kind gift from David Chan, California Institute of Technology, Pasadena, CA. Oligodeoxynucleotides were synthesized and HPLC-purified by Integrated DNA Technologies.

Electrophoretic Mobility-Shift Assays. Six-microliter solutions containing 20 mM Hepes (pH 7.4), 90 mM NaCl, 20 mM EDTA, 4 μM dsDNA, and varying concentrations of TFAM were assembled on ice and allowed to equilibrate at room temperature for 1 h. The solution was mixed with 0.6 μL of 10× loading buffer (40% glycerol with bromophenol blue and xylene-cyanol). Electrophoresis was performed on a 6% native polyacrylamide gel at 100 V and 4 °C. The gel image was acquired on a Typhoon FLA7000 (GE Healthcare) imager followed by quantification using ImageQuant software. Data were analyzed using GraphPad Prism v6.0.

Preparation of AP-DNA. AP lesion-containing DNA was prepared from a site-specifically modified oligodeoxynucleotide containing a deoxyuridine residue. The dU residues were converted to AP sites upon digestion with uracil-DNA glycosylase (New England Biolabs). Briefly, for 6 h at 37 °C, 3 nmol of the dU-containing oligomer was incubated with 6 units of UDG in a buffer containing 20 mM Tris·HCl (pH 8.0 at 25 °C), 1 mM DTT, and 1 mM EDTA. The completion of the reaction was confirmed by converting AP-DNA into single-stranded breaks upon alkaline cleavage (0.1 M NaOH at 37 °C for 1 h) and analyzing cleavage products by denaturing PAGE. The AP-DNA was purified by phenol/chloroform extraction and stored at −80 °C. The AP-harboring dsDNA substrates were prepared by annealing the AP-containing ssDNA with a complementary strand at 65 °C for 15 min followed by slow cooling overnight.

Reactions of TFAM with AP-DNA. AP-DNA was incubated with TFAM to monitor the rates of strand scission and SSB and DPC formation. Reactions contained 4 μM AP-DNA, 8 μM TFAM, 20 mM Hepes (pH 7.4), 90 mM NaCl, and 20 mM EDTA, with or without 25 mM $NaBH_3CN$. Reactions were conducted at 37 °C, with aliquots taken at varying times. The aliquots were quenched by adding an equal volume of 0.2 M $NaBH_4$ and rapid cooling on ice. The samples were stored at −80 °C before electrophoretic analysis. For SDS-urea PAGE, the quenched reactions were mixed with a gel loading solution containing 95% (vol/vol) formamide, 50 mM EDTA, and 1% SDS, and analyzed on an 8- × 10-cm SDS-urea (7 M) PAGE (16%) gel. For denaturing PAGE analysis, the quenched samples were digested with trypsin (5 mg/mL, 37 °C for 2 h), followed by mixing with a 1.5 volume of loading solution containing 95% (vol/vol) formamide and 50 mM EDTA for electrophoresis (18% polyacrylamide/bis-acrylamide [19:1], 7 M urea, 38 × 30 cm). The apparent DNA disappearance rate was obtained by fitting the percent of intact DNA to a single-exponential function.

Reactions of AP-DNA with Mitochondrial Extracts. Mitochondrial extracts were prepared from 5×10^6 HeLa cells using components from a mitochondrial DNA isolation kit (BioVision). Briefly, cell pellets were suspended in a cytosol extraction buffer and incubated on ice for 10 min. Cells were lysed in an ice-cold Dounce homogenizer (50 passes). The lysate was clarified by centrifugation at 700 × *g* for 10 min at 4 °C. The supernatant containing intact mitochondria was washed twice with a cytosol extraction buffer followed by centrifugation at 10,000 × *g* for 30 min at 4 °C. The isolated mitochondria were lysed with 30 μL of lysis buffer on ice for 10 min in the presence of protease inhibitor mixture before flash-freezing with liquid nitrogen in small aliquots. Mitochondrial extracts from HEK-293 cells were prepared following the same procedure using 1×10^7 cells. Reactions of AP-DNA with mitochondrial extracts contained 4 μM AP_{15}, 1.5 μL mitochondrial extracts, 25 mM $NaBH_3CN$, 20 mM Hepes (pH 7.4), and 20 mM EDTA in the presence of protease inhibitor mixture. The reaction mixture was incubated for 1 h at 37 °C, before quenching with 3 volumes of the stop solution containing 0.1 M $NaBH_4$, 0.2% SDS, 0.15 M β-mercaptoethanol, and 90% formamide. The quenched solution was denatured at 90 °C for 10 min followed by rapid cooling on ice. Reaction products were analyzed on an SDS/PAGE gel (4 to 20%; Bio-Rad). Free and cross-linked TFAM were detected using Western blotting analysis with a primary mouse anti-human TFAM antibody (Santa Cruz Biotechnology) and a secondary HRP-conjugated goat anti-mouse IgG antibody (Novus Biologicals). Gel images were developed in Clarity Western ECL Substrate (Bio-Rad) and obtained on a ChemiDoc Touch Imaging System (Bio-Rad).

Reactions of AP-DNA with APE1. The AP lyase activity of APE1 in mitochondrial extracts was assayed using a THF-containing DNA substrate (AP_{15}-THF; sequence shown in *SI Appendix*, Table S1) (47, 66). Reactions contained 5 μM AP_{15}-THF, 3 μL mitochondrial extracts, 0.2 mM EDTA, 20 mM Hepes (pH 7.4), and 5 mM $MgCl_2$ in the presence of protease inhibitor mixture. Reactions were allowed for 10 min at 37 °C and stopped by adding a 1.5 volume of quench solution containing 90% (vol/vol) formamide, 50 mM EDTA, 0.2% SDS, and 0.15 M β-mercaptoethanol. APE1-cleaved DNA products were verified by comparing products from reactions containing mitochondrial extracts with that of a similar reaction with recombinant APE1 (5 nM). To examine the inhibitory effect of TFAM toward APE1 lyase activity, reactions were performed using 1 μM AP_{15}-THF, 1 nM (or 10 or 100 nM) APE1, 20 mM Hepes (pH 7.4), 90 mM NaCl, 100 μg/mL BSA, 0.25 mM EDTA, and 5 mM $MgCl_2$ with varying concentrations of TFAM (0.1, 0.5, 0.7, 0.9, 1.1, 2.1, 2.7, 3.6, 4.8, 6.0, 8.0, or 10 μM). Reactions were quenched by mixing a 2-μL reaction aliquot with 8 μL loading dye containing 50 mM EDTA and 90% formamide followed by denaturing PAGE analysis. APE1 activity was defined as the percentage of the cleaved DNA product (6 nt). Relative IC_{50} was obtained by fitting the data to the following equation using GraphPad Prism v6.0.

$$y = y_{min} + \frac{(y_{max} - y_{min})}{1 + 10^{n\cdot(logIC_{50} - x)}},$$

where *x* is the concentration of TFAM and *y* is the APE1 activity, as defined by the percentage of cleaved product DNA relative to the sum intensity of substrate and product.

ACKNOWLEDGMENTS. We thank Dr. Laurie Kaguni for critically reading the manuscript, Dr. David Chan for providing the expression vector of human TFAM, Dr. Yinsheng Wang for providing shRNA-mediated TFAM stable knockdown HeLa cells, Wenxin Zhao for performing several TFAM–AP-DNA reactions, and Daniel Oppong for assisting with APE1 expression. This work was supported by National Institutes of Health Grant R35 GM128854 (to L.Z.), Central Michigan University startup funds, and a Faculty Research and Creative Endeavor Award.

1. L. Galluzzi, O. Kepp, G. Kroemer, Mitochondria: Master regulators of danger signalling. *Nat. Rev. Mol. Cell Biol.* **13**, 780–788 (2012).
2. J. Nunnari, A. Suomalainen, Mitochondria: In sickness and in health. *Cell* **148**, 1145–1159 (2012).
3. M. Alexeyev, I. Shokolenko, G. Wilson, S. LeDoux, The maintenance of mitochondrial DNA integrity—Critical analysis and update. *Cold Spring Harb. Perspect. Biol.* **5**, a012641 (2013).
4. C. M. Gustafsson, M. Falkenberg, N.-G. Larsson, Maintenance and expression of mammalian mitochondrial DNA. *Annu. Rev. Biochem.* **85**, 133–160 (2016).
5. M. Scheibye-Knudsen, E. F. Fang, D. L. Croteau, D. M. Wilson, III, V. A. Bohr, Protecting the mitochondrial powerhouse. *Trends Cell Biol.* **25**, 158–170 (2015).
6. B. Van Houten, S. E. Hunter, J. N. Meyer, Mitochondrial DNA damage induced autophagy, cell death, and disease. *Front. Biosci.* **21**, 42–54 (2016).
7. W. C. Copeland, M. J. Longley, Mitochondrial genome maintenance in health and disease. *DNA Repair (Amst.)* **19**, 190–198 (2014).
8. O. Russell, D. Turnbull, Mitochondrial DNA disease—Molecular insights and potential routes to a cure. *Exp. Cell Res.* **325**, 38–43 (2014).
9. M. J. Keogh, P. F. Chinnery, Mitochondrial DNA mutations in neurodegeneration. *Biochim. Biophys. Acta* **1847**, 1401–1411 (2015).
10. A. Stein, E. A. Sia, Mitochondrial DNA repair and damage tolerance. *Front. Biosci.* **22**, 920–943 (2017).
11. M. Muftuoglu, M. P. Mori, N. C. de Souza-Pinto, Formation and repair of oxidative damage in the mitochondrial DNA. *Mitochondrion* **17**, 164–181 (2014).
12. A. Prakash, S. Doublié, Base excision repair in the mitochondria. *J. Cell. Biochem.* **116**, 1490–1499 (2015).
13. J. A. Swenberg *et al.*, Endogenous versus exogenous DNA adducts: Their role in carcinogenesis, epidemiology, and risk assessment. *Toxicol. Sci.* **120** (suppl. 1), S130–S145 (2011).
14. J. Nakamura *et al.*, The endogenous exposome. *DNA Repair (Amst.)* **19**, 3–13 (2014).
15. J. Hegler, D. Bittner, S. Boiteux, B. Epe, Quantification of oxidative DNA modifications in mitochondria. *Carcinogenesis* **14**, 2309–2312 (1993).
16. P. K. Mishra *et al.*, Mitochondrial oxidative stress-induced epigenetic modifications in pancreatic epithelial cells. *Int. J. Toxicol.* **33**, 116–129 (2014).

17. F. Legros, F. Malka, P. Frachon, A. Lombès, M. Rojo, Organization and dynamics of human mitochondrial DNA. *J. Cell Sci.* **117**, 2653–2662 (2004).
18. M. M. Greenberg, Abasic and oxidized abasic site reactivity in DNA: Enzyme inhibition, cross-linking, and nucleosome catalyzed reactions. *Acc. Chem. Res.* **47**, 646–655 (2014).
19. S. Dutta, G. Chowdhury, K. S. Gates, Interstrand cross-links generated by abasic sites in duplex DNA. *J. Am. Chem. Soc.* **129**, 1852–1853 (2007).
20. N. E. Price *et al*., Interstrand DNA-DNA cross-link formation between adenine residues and abasic sites in duplex DNA. *J. Am. Chem. Soc.* **136**, 3483–3490 (2014).
21. L. Guan, M. M. Greenberg, Irreversible inhibition of DNA polymerase β by an oxidized abasic lesion. *J. Am. Chem. Soc.* **132**, 5004–5005 (2010).
22. J. T. Sczepanski, R. S. Wong, J. N. McKnight, G. D. Bowman, M. M. Greenberg, Rapid DNA-protein cross-linking and strand scission by an abasic site in a nucleosome core particle. *Proc. Natl. Acad. Sci. U.S.A.* **107**, 22475–22480 (2010).
23. L. Guan, K. Bebenek, T. A. Kunkel, M. M. Greenberg, Inhibition of short patch and long patch base excision repair by an oxidized abasic site. *Biochemistry* **49**, 9904–9910 (2010).
24. L. A. Loeb, B. D. Preston, Mutagenesis by apurinic/apyrimidinic sites. *Annu. Rev. Genet.* **20**, 201–230 (1986).
25. V. Simonelli, L. Narciso, E. Dogliotti, P. Fortini, Base excision repair intermediates are mutagenic in mammalian cells. *Nucleic Acids Res.* **33**, 4404–4411 (2005).
26. N. E. Price, L. Li, K. S. Gates, Y. Wang, Replication and repair of a reduced 2′-deoxyguanosine-abasic site interstrand cross-link in human cells. *Nucleic Acids Res.* **45**, 6486–6493 (2017).
27. I. Shokolenko, N. Venediktova, A. Bochkareva, G. L. Wilson, M. F. Alexeyev, Oxidative stress induces degradation of mitochondrial DNA. *Nucleic Acids Res.* **37**, 2539–2548 (2009).
28. A. M. Furda, A. M. Marrangoni, A. Lokshin, B. Van Houten, Oxidants and not alkylating agents induce rapid mtDNA loss and mitochondrial dysfunction. *DNA Repair (Amst.)* **11**, 684–692 (2012).
29. I. N. Shokolenko, G. L. Wilson, M. F. Alexeyev, Persistent damage induces mitochondrial DNA degradation. *DNA Repair (Amst.)* **12**, 488–499 (2013).
30. I. N. Shokolenko, G. L. Wilson, M. F. Alexeyev, The "fast" and the "slow" modes of mitochondrial DNA degradation. *Mitochondrial DNA A DNA Mapp. Seq. Anal.* **27**, 490–498 (2016).
31. I. N. Shokolenko, M. F. Alexeyev, Mitochondrial DNA: A disposable genome? *Biochim. Biophys. Acta. Mol. Basis Dis.* **1852**, 1805–1809 (2015).
32. A. Moretton *et al*., Selective mitochondrial DNA degradation following double-strand breaks. *PLoS One* **12**, e0176795 (2017).
33. A. Mansouri, C. Demeilliers, S. Amsellem, D. Pessayre, B. Fromenty, Acute ethanol administration oxidatively damages and depletes mitochondrial DNA in mouse liver, brain, heart, and skeletal muscles: Protective effects of antioxidants. *J. Pharmacol. Exp. Ther.* **298**, 737–743 (2001).
34. M. Pinto, C. T. Moraes, Mechanisms linking mtDNA damage and aging. *Free Radic. Biol. Med.* **85**, 250–258 (2015).
35. S. Oka *et al*., Two distinct pathways of cell death triggered by oxidative damage to nuclear and mitochondrial DNAs. *EMBO J.* **27**, 421–432 (2008).
36. N. Kozhukhar, D. Spadafora, R. Fayzulin, I. N. Shokolenko, M. Alexeyev, The efficiency of the translesion synthesis across abasic sites by mitochondrial DNA polymerase is low in mitochondria of 3T3 cells. *Mitochondrial DNA A DNA Mapp. Seq. Anal.* **27**, 4390–4396 (2016).
37. H. B. Ngo, J. T. Kaiser, D. C. Chan, The mitochondrial transcription and packaging factor Tfam imposes a U-turn on mitochondrial DNA. *Nat. Struct. Mol. Biol.* **18**, 1290–1296 (2011).
38. A. Rubio-Cosials *et al*., Human mitochondrial transcription factor A induces a U-turn structure in the light strand promoter. *Nat. Struct. Mol. Biol.* **18**, 1281–1289 (2011).
39. H. B. Ngo, G. A. Lovely, R. Phillips, D. C. Chan, Distinct structural features of TFAM drive mitochondrial DNA packaging versus transcriptional activation. *Nat. Commun.* **5**, 3077 (2014).
40. C. Kukat *et al*., Cross-strand binding of TFAM to a single mtDNA molecule forms the mitochondrial nucleoid. *Proc. Natl. Acad. Sci. U.S.A.* **112**, 11288–11293 (2015).
41. D. Barsky, N. Foloppe, S. Ahmadia, D. M. Wilson, III, A. D. MacKerell, Jr, New insights into the structure of abasic DNA from molecular dynamics simulations. *Nucleic Acids Res.* **28**, 2613–2626 (2000).
42. J. Chen, F.-Y. Dupradeau, D. A. Case, C. J. Turner, J. Stubbe, DNA oligonucleotides with A, T, G or C opposite an abasic site: Structure and dynamics. *Nucleic Acids Res.* **36**, 253–262 (2008).
43. C. Zhou, J. T. Sczepanski, M. M. Greenberg, Mechanistic studies on histone catalyzed cleavage of apyrimidinic/apurinic sites in nucleosome core particles. *J. Am. Chem. Soc.* **134**, 16734–16741 (2012).
44. A. Rubio-Cosials *et al*., Protein flexibility and synergy of HMG domains underlie U-turn bending of DNA by TFAM in solution. *Biophys. J.* **114**, 2386–2396 (2018).
45. R. Chattopadhyay *et al*., Identification and characterization of mitochondrial abasic (AP)-endonuclease in mammalian cells. *Nucleic Acids Res.* **34**, 2067–2076 (2006).
46. A. Gelin *et al*., Genetic and biochemical characterization of human AP endonuclease 1 mutants deficient in nucleotide incision repair activity. *PLoS One* **5**, e12241 (2010).
47. Z. Sevilya *et al*., Development of APE1 enzymatic DNA repair assays: Low APE1 activity is associated with increase lung cancer risk. *Carcinogenesis* **36**, 982–991 (2015).
48. F. Hensen, S. Cansiz, J. M. Gerhold, J. N. Spelbrink, To be or not to be a nucleoid protein: A comparison of mass-spectrometry based approaches in the identification of potential mtDNA-nucleoid associated proteins. *Biochimie* **100**, 219–226 (2014).
49. S. Han *et al*., Proximity biotinylation as a method for mapping proteins associated with mtDNA in living cells. *Cell Chem. Biol.* **24**, 404–414 (2017).
50. C. Takamatsu *et al*., Regulation of mitochondrial D-loops by transcription factor A and single-stranded DNA-binding protein. *EMBO Rep.* **3**, 451–456 (2002).
51. C. Kukat *et al*., Super-resolution microscopy reveals that mammalian mitochondrial nucleoids have a uniform size and frequently contain a single copy of mtDNA. *Proc. Natl. Acad. Sci. U.S.A.* **108**, 13534–13539 (2011).
52. N. J. Gross, G. S. Getz, M. Rabinowitz, Apparent turnover of mitochondrial deoxyribonucleic acid and mitochondrial phospholipids in the tissues of the rat. *J. Biol. Chem.* **244**, 1552–1562 (1969).
53. W. J. Driggers, G. P. Holmquist, S. P. LeDoux, G. L. Wilson, Mapping frequencies of endogenous oxidative damage and the kinetic response to oxidative stress in a region of rat mtDNA. *Nucleic Acids Res.* **25**, 4362–4369 (1997).
54. Y. Kai *et al*., Rapid and random turnover of mitochondrial DNA in rat hepatocytes of primary culture. *Mitochondrion* **6**, 299–304 (2006).
55. L. L. Clay Montier, J. J. Deng, Y. Bai, Number matters: Control of mammalian mitochondrial DNA copy number. *J. Genet. Genomics* **36**, 125–131 (2009).
56. A. Rötig, J. Poulton, Genetic causes of mitochondrial DNA depletion in humans. *Biochim. Biophys. Acta* **1792**, 1103–1108 (2009).
57. T. Oka *et al*., Mitochondrial DNA that escapes from autophagy causes inflammation and heart failure. *Nature* **485**, 251–255 (2012).
58. Q. Zhang *et al*., Circulating mitochondrial DAMPs cause inflammatory responses to injury. *Nature* **464**, 104–107 (2010).
59. S. R. Bacman, S. L. Williams, M. Pinto, S. Peralta, C. T. Moraes, Specific elimination of mutant mitochondrial genomes in patient-derived cells by mitoTALENs. *Nat. Med.* **19**, 1111–1113 (2013).
60. P. A. Gammage, J. Rorbach, A. I. Vincent, E. J. Rebar, M. Minczuk, Mitochondrially targeted ZFNs for selective degradation of pathogenic mitochondrial genomes bearing large-scale deletions or point mutations. *EMBO Mol. Med.* **6**, 458–466 (2014).
61. P. Reddy *et al*., Selective elimination of mitochondrial mutations in the germline by genome editing. *Cell* **161**, 459–469 (2015).
62. S. R. Bacman *et al*., MitoTALEN reduces mutant mtDNA load and restores $tRNA^{Ala}$ levels in a mouse model of heteroplasmic mtDNA mutation. *Nat. Med.* **24**, 1696–1700 (2018).
63. G. Farge *et al*., Protein sliding and DNA denaturation are essential for DNA organization by human mitochondrial transcription factor A. *Nat. Commun.* **3**, 1013 (2012).
64. N. Nissanka, S. R. Bacman, M. J. Plastini, C. T. Moraes, The mitochondrial DNA polymerase gamma degrades linear DNA fragments precluding the formation of deletions. *Nat. Commun.* **9**, 2491 (2018).
65. V. Peeva *et al*., Linear mitochondrial DNA is rapidly degraded by components of the replication machinery. *Nat. Commun.* **9**, 1727 (2018).
66. C. Canugovi *et al*., The mitochondrial transcription factor A functions in mitochondrial base excision repair. *DNA Repair (Amst.)* **9**, 1080–1089 (2010).
67. Y. Matsushima, Y. Goto, L. S. Kaguni, Mitochondrial Lon protease regulates mitochondrial DNA copy number and transcription by selective degradation of mitochondrial transcription factor A (TFAM). *Proc. Natl. Acad. Sci. U.S.A.* **107**, 18410–18415 (2010).
68. B. Lu *et al*., Phosphorylation of human TFAM in mitochondria impairs DNA binding and promotes degradation by the AAA+ Lon protease. *Mol. Cell* **49**, 121–132 (2013).
69. G. A. King *et al*., Acetylation and phosphorylation of human TFAM regulate TFAM-DNA interactions via contrasting mechanisms. *Nucleic Acids Res.* **46**, 3633–3642 (2018).